RESEARCH ARTICLE | AUGUST 02 2024

Sequence and gelation in supramolecular polymers **⊘**

Christopher Balzer ⊚ ; Glenn H. Fredrickson ■ ◎



J. Chem. Phys. 161, 054907 (2024) https://doi.org/10.1063/5.0218748

A CHORUS





Articles You May Be Interested In

Humidity affects the viscoelastic properties of supramolecular living polymers

J. Rheol. (November 2017)

Coherent states field theory in supramolecular polymer physics

J. Chem. Phys. (May 2018)

Field-theoretic model of inhomogeneous supramolecular polymer networks and gels

J. Chem. Phys. (November 2010)





Sequence and gelation in supramolecular polymers

Cite as: J. Chem. Phys. 161, 054907 (2024); doi: 10.1063/5.0218748

Submitted: 13 May 2024 · Accepted: 20 July 2024 ·

Published Online: 2 August 2024









Christopher Balzer¹ o and Glenn H. Fredrickson^{1,2,a)}



AFFILIATIONS

- Materials Research Laboratory, University of California, Santa Barbara, California 93106, USA
- ²Departments of Chemical Engineering and Materials, University of California, Santa Barbara, California 93106, USA
- a) Author to whom correspondence should be addressed: ghf@ucsb.edu

ABSTRACT

Supramolecular polymer networks exhibit unique and tunable thermodynamic and dynamic properties that are attractive for a wide array of applications, such as adhesives, rheology modifiers, and compatibilizers. Coherent states (CS) field theories have emerged as a powerful approach for describing the possibly infinite reaction products that result from associating polymers. Up to this point, CS theories have focused on relatively simple polymer architectures. In this work, we develop an extension of the CS framework to study polymers with reversible bonds distributed along the polymer backbone, opening a broad array of new materials that can be studied with theoretical methods. We use this framework to discern the role of reactive site placement on sol-gel phase behavior, including the prediction of a microstructured gel phase that has not been reported for neutral polymer gels. Our results highlight the subtleties of thermodynamics in supramolecular polymers and the necessity for theories that capture them.

Published under an exclusive license by AIP Publishing. https://doi.org/10.1063/5.0218748

I. INTRODUCTION

Supramolecular polymers reversibly bond to other polymer chains via non-covalent linkages, such as hydrogen bonding, π - π interactions, or electrostatic interactions. ¹⁻³ The reversible nature of the interactions enables a variety of stimuli responsiveness and selfassembly behavior, leading to their use as flow modifiers, self-healing polymers, and compatibilizers, among other applications.

Gelation is a fundamental phenomenon in supramolecular polymer materials. Network formation connects molecular-level linkages to macroscopic viscoelastic properties. Theoretical descriptions of gelation in polymer systems go back to the 1940s with Flory and Stockmayer, 9,10 who first quantified the gel point and created a connection between the molecular weight distribution and macroscopic gel properties. In the time since, molecularly informed theories of polymer systems have been successful in describing gel swelling, 11-13 deformation, 14-16 and thermodynamics. 17,18 However, a persistent challenge in the theory of reacting polymer systems is enumerating all (possibly infinite) distributions of reaction products.

Efforts to overcome this challenge typically make assumptions about the reaction product structure. Using a combinatoric argument of N_p "stickers" on each chain reacting with probability p, Semenov and Rubinstein developed the first quantitative model for the phase behavior of thermoreversible gels, 9 establishing that the formation of a reversible network is always associated with phase separation. Formulated at the mean-field level, their theory does not take into account the position of stickers on the polymer chains or the correlations that arise from the positions of stickers. Recently, Danielsen augmented the Semenov and Rubinstein theory by approximating linkages between chains as effective 4-arm polymer stars, omitting the effect of higher-order branched species and loops, to study the role of reactive site spacing, among other factors, in the phase behavior in hetero-associating polymer blends.²⁰ In an auxiliary-field framework, Mohan, Elliot, and Fredrickson developed an inhomogeneous theory of gelation for a system consisting of purely tree-like structures, which allowed them to enumerate infinite isomers.^{21,22} Their theory is consistent with Flory and Stockmayer formalism as well as the other mean-field approaches in the homogeneous limit. Rabin and Panyukov derived a comprehensive theory of gelation using a framework known as replica field theory that utilizes the so-called " $n \to 0$ " trick,²³ and their theory has been instrumental in understanding and quantifying inhomogeneities in gels. Each of the works above has been successful in its own right, but the necessary simplification of reaction products or the theoretical approach limits the applicability of the theories beyond the mean-field.

The coherent states (CSs) polymer field theory framework is a theoretical method that avoids the central issue of describing reaction products. 24-26 Instead of enumerating possible products, polymer chains are built from stochastically evaluated chain propagators that inherently generate all possible reaction species.²⁷ Importantly, the resulting field theory can be numerically evaluated using well-established complex Langevin schemes to sample fluctuations beyond mean-field. So far, the CS framework has been used to study relatively simple supramolecular architectures, such as end-functionalized polymers with equivalent reaction sites. 27,29 CS theories currently lack the flexibility to explore systems with arbitrary reactive site positions, a factor that molecular dynamics simulations demonstrate plays a key role in phase behavior. 30,31 Moreover, precise synthesis techniques now allow for nearly arbitrary placement of reaction sites along a polymer backbone or on side chains. 32-37 A predictive theory that accounts for the diversity of supramolecular polymers is necessary to navigate such a large design

To that end, the focus of this work is to extend the coherent states framework to describe arbitrarily placed reaction sites in supramolecular polymers. Our resulting theory can be used to study multiple reaction types and multi-component and, since it is formulated in the CS framework, is amenable to direct numerical simulation. As we will show, the theoretical approach elegantly imbues reactivity along a polymer chain by effectively tagging reactive sites with a local field ψ^* . The tagging process naturally connects abstract field variables to physically relevant thermodynamic quantities, such as reaction conversion. We introduce and demonstrate the theory in the context of reversible network gelation in a good solvent. The mean-field limit of our theory is compared to previous theories of gelation. At the level of the random phase approximation, we study the effect of reactive site placement on gelation and, in doing so, demonstrate novel phase behavior in neutral gels. Namely, a microstructured gel region appears within the typical sol-gel phase diagram. The physical origin of the microstructured gel is sequenceinduced correlations that manifest as clustering of bonds between polymer chains. These results indicate that there is rich phase behavior related to the coupling between monomer type (differing by reactivity, chemical composition, etc.) and their arrangement on the polymer backbone.

II. THEORETICAL MODEL

The central goal of the current work is to account for non-equivalent reaction sites in polymer coherent states models. As mentioned earlier, previous coherent states approaches have utilized the symmetry in polymer architecture to simplify the theoretical form. For an arbitrary number of reactive sites and placements, the number of pairwise reactions of M functional groups is M!/[2(M-2)!]. While it is possible to enumerate each pairwise term, accessing thermodynamic information such as the reaction conversion is tedious with many individual reaction terms. An elegant and transferable approach is to tag each segment-level reactive site with a local field that encompasses all reactive groups distributed along the polymer chain. We will derive this approach for discrete Gaussian chains in a

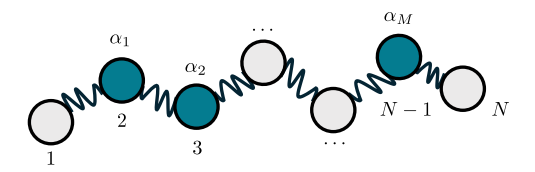


FIG. 1. Graphic of bead-spring polymer with N beads and M reactive sites. Reactive sites are denoted by their index along the polymer backbone $\{\alpha_1, \alpha_2, \ldots, \alpha_{M-1}, \alpha_M\}$.

so-called hybrid coherent states theory, and then we take the continuous Gaussian chain limit to arrive at a pure coherent states theory for non-equivalent reaction sites.

Consider a bead-spring model for linear polymers in an implicit solvent, each with N total beads and M functional groups distributed along the backbone at contour positions $\{\alpha_1,\alpha_2,\ldots,\alpha_M\}$ (Fig. 1). To focus on backbone functionalization, we will assume the reactive groups are not at the ends of the chain. Incorporating end-functionalization is a straight-forward extension. In a hybrid auxiliary-field and coherent states framework, 28 the canonical partition function is

$$Z(n, M, V, T) = \frac{Z_0}{D_w D_\phi} \int \mathcal{D}w \int \mathcal{D}(\phi^*, \phi) \ e^{-H[w, \phi^*, \phi]}, \quad (1)$$

where $Z_0 = \bar{V}^n/n!$ is the ideal partition function for n polymer chains in a reduced volume $\bar{V} = V/R_{g_0}^3$ and D_w and D_ϕ are normalizing Gaussian integrals.²⁸ $R_{g_0} = (N/6)^{1/2}b$ is the unperturbed radius of gyration with segment length b. The effective Hamiltonian is

$$H = \frac{1}{2u_0} \int d\mathbf{r} \ w(\mathbf{r})^2 + \sum_{j=1}^N \int d\mathbf{r} \ \phi_j^*(\mathbf{r}) \phi_j(\mathbf{r})$$
$$- \sum_{j=2}^N \int d\mathbf{r} \ \phi_j^*(\mathbf{r}) e^{-iw(\mathbf{r})} \Phi(\mathbf{r}) * \phi_{j-1}(\mathbf{r})$$
$$- \int d\mathbf{r} \ \phi_1^*(\mathbf{r}) e^{-iw(\mathbf{r})} - n \ln\left(\frac{1}{V} \int d\mathbf{r} \ \phi_N(\mathbf{r})\right) + H_{\text{rxn}}, \tag{2}$$

where u_0 is the excluded volume interaction parameter between monomers, * represents a spatial convolution, and $\Phi(\mathbf{r})$ is a normalized linking function that embeds the backbone bonding potential between successive polymer beads.

The first term in H accounts for the non-bonded interactions with $u_0 > 0$ corresponding to a good solvent, the second and third terms serve to propagate polymer chains, and the fourth and fifth terms are source and sink terms that initiate polymers at index 1 and terminate n polymer chains at index N, respectively. The final term in the Hamiltonian is responsible for building all of the products of reversible reactions. With M reactive sites of the same type, the form is

$$H_{\text{rxn}} = \frac{\lambda}{2} \sum_{m=1}^{M} \sum_{n=1}^{M} \int d\mathbf{r} \int d\mathbf{r}' \Big(\phi_{\alpha_{m}}^{*}(\mathbf{r}) e^{-iw(\mathbf{r})} \Phi(\mathbf{r}) * \phi_{\alpha_{m}-1}(\mathbf{r}) \Big)$$

$$\times R(\mathbf{r}, \mathbf{r}') \Big(\phi_{\alpha_{n}}^{*}(\mathbf{r}') e^{-iw(\mathbf{r}')} \Phi(\mathbf{r}') * \phi_{\alpha_{n}-1}(\mathbf{r}') \Big), \tag{3}$$

where λ is the bond strength and is related to the equilibrium constant for the pairing reaction, and $R(\mathbf{r}, \mathbf{r}')$ is a bonding or reaction kernel. The $\phi_{\alpha_m}^*(\mathbf{r})e^{-iw(\mathbf{r})}\Phi(\mathbf{r})*\phi_{\alpha_m-1}(\mathbf{r})$ terms in Eq. (3) are

the statistical weights of a bead at index α_m being connected to the previous bead $\alpha_m - 1$ at position \mathbf{r} . Pairing two such sites via the reaction kernel encodes bonding. $R(\mathbf{r}, \mathbf{r}')$ can take the form of any bonding potential, but the simplest choice is a Dirac delta function.

The non-local and bilinear form of Eq. (3) is not convenient for further analytical manipulation or for efficient computation—all of the reaction information is spread out across the chain. Instead, we can tag all of the fields by wrapping them into a single field $\psi(\mathbf{r})$ through an identity transformation, $\int \mathcal{D}\psi \ \delta\Big(\psi(\mathbf{r}) - \sum_{m=1}^{M} \phi_{\alpha_m}^*(\mathbf{r}) e^{-iw(\mathbf{r})} \Phi(\mathbf{r}) * \phi_{\alpha_m-1}(\mathbf{r})\Big) = 1.$ Using the Fourier representation of the delta function to introduce another local field ψ^* results in the following partition function:

$$Z(n, M, V, T) = \frac{Z_0}{D_w D_\phi D_\psi} \int \mathcal{D}w \int \mathcal{D}(\phi^*, \phi)$$

$$\times \int \mathcal{D}(\psi^*, \psi) e^{-H[w, \phi^*, \phi, \psi^*, \psi]}, \qquad (4)$$

where D_{ψ} is a normalizing Gaussian integral. The effective Hamiltonian becomes

$$H = \frac{1}{2u_0} \int d\mathbf{r} \ w(\mathbf{r})^2 + \sum_{j=1}^{N} \int d\mathbf{r} \ \phi_j^*(\mathbf{r}) \phi_j(\mathbf{r})$$

$$- \sum_{j=2}^{N} \int d\mathbf{r} \ \phi_j^*(\mathbf{r}) e^{-iw(\mathbf{r})} \Phi(\mathbf{r}) * \phi_{j-1}(\mathbf{r})$$

$$- \sum_{m=1}^{M} \int d\mathbf{r} \ \phi_m^*(\mathbf{r}) e^{-iw(\mathbf{r})} (\psi^*(\mathbf{r}) - 1) \Phi(\mathbf{r}) * \phi_{m-1}(\mathbf{r})$$

$$- \int d\mathbf{r} \ \phi_1^*(\mathbf{r}) e^{-iw(\mathbf{r})} - n \ln \left(\frac{1}{V} \int d\mathbf{r} \ \phi_N(\mathbf{r}) \right)$$

$$+ \int d\mathbf{r} \left[\psi^*(\mathbf{r}) \psi(\mathbf{r}) - \psi(\mathbf{r}) - \frac{\lambda}{2} \psi(\mathbf{r}) \int d\mathbf{r}' R(\mathbf{r}, \mathbf{r}') \psi(\mathbf{r}') \right]. (5)$$

Comparing Eq. (5) to Eq. (2), we can see that propagation terms for reactive sites include a factor of ψ^* , which serves to functionalize beads. The final line of Eq. (5) encompasses all of the reactions with $\psi^*\psi$ linking the relevant fields and ψ and $\frac{\lambda}{2}\psi(\mathbf{r})\int d\mathbf{r}' R(\mathbf{r},\mathbf{r}')\psi(\mathbf{r}')$ either leaving a site unreacted or bonded to another reactive site, respectively. The key advantages of this framework are that the fields ψ and ψ^* are local, and one can assign reactivity by simply placing a factor of ψ^* on reactive monomers. Furthermore, important thermodynamic properties are now connected to the ψ and ψ^* fields. For instance, the average density of bonds²⁷ is given by

$$\rho_{\text{bond}} = \frac{1}{V} \frac{\partial \ln Z}{\partial \ln \lambda} = \frac{\lambda}{2V} \int d\mathbf{r} \left\{ \psi(\mathbf{r}) \int d\mathbf{r}' \ R(\mathbf{r}, \mathbf{r}') \psi(\mathbf{r}') \right\}, \quad (6)$$

where the angled brackets denote the ensemble average with statistical weight $e^{-H\left[w,\phi^*,\phi,\psi^*,\psi\right]}$. The average conversion is $\eta=\frac{2\rho_{\rm bond}}{MC}$, where $C=n/\bar{V}$ is the reduced chain density.

The theory presented earlier becomes more compact for continuous Gaussian chains. Instead of discrete beads referenced by an integer index *j*, the chain is represented as a line contour, and both fields vary continuously over a chain contour variable *s*. Reactive sites are represented as points along the chain contour. Upon taking

the limit of continuous Gaussian chains, we can convert the theory to a pure coherent states theory. 28 The resulting partition function is

$$Z(n, M, V, T) = \frac{Z_0}{D_{\phi}D_{\psi}} \int \mathcal{D}(\phi^*, \phi) \int \mathcal{D}(\psi^*, \psi) e^{-H[\phi^*, \phi, \psi^*, \psi]}. \quad (7)$$

The effective Hamiltonian is

$$H = \frac{1}{2} \int d\mathbf{r} \int d\mathbf{r}' \, \tilde{\rho}(\mathbf{r}) u(\mathbf{r}, \mathbf{r}') \tilde{\rho}(\mathbf{r}')$$

$$+ \int_{0}^{N} ds \int d\mathbf{r} \, \phi^{*}(\mathbf{r}, s+) \, \mathcal{L}\phi(\mathbf{r}, s)$$

$$- \sum_{m=1}^{M} \int d\mathbf{r} \, \phi^{*}(\mathbf{r}, s_{m}^{+}) \phi(\mathbf{r}, s_{m}^{-}) (\psi^{*}(\mathbf{r}) - 1)$$

$$- \int d\mathbf{r} \, \phi^{*}(\mathbf{r}, 0) - n \ln \left(\frac{1}{V} \int d\mathbf{r} \, \phi(\mathbf{r}, N) \right)$$

$$+ \int d\mathbf{r} \left[\psi^{*}(\mathbf{r}) \psi(\mathbf{r}) - \psi(\mathbf{r}) - \frac{\lambda}{2} \psi(\mathbf{r}) \int d\mathbf{r}' \, R(\mathbf{r}, \mathbf{r}') \psi(\mathbf{r}') \right], \tag{8}$$

where $\mathcal{L} = \partial/\partial s - (b/6)\nabla^2$ is the chain diffusion operator, $\tilde{\rho}(\mathbf{r}) = \int_0^N ds \phi^*(\mathbf{r},s+)\phi(\mathbf{r},s)$ is the density operator, and $u(\mathbf{r},\mathbf{r}')$ is the nonbonded pair interaction potential in units of k_BT between polymer segments. The argument of s+ indicates that ϕ^* fields are evaluated at an infinitesimally larger argument in order to generate the correct causal response.²⁸ In the continuous chain theory, the reactive sites essentially appear as source/sink terms paired with a factor $\psi^* - 1$.

The CS framework is flexible in that there are several ways to represent the canonical ensemble. 28 Without derivation, we can equivalently represent the source/sink terms in the continuous chain theory as

$$H_{S} = -n \ln \left(\frac{1}{V^{M}} \prod_{m=1}^{M} \int d\mathbf{r} \, \phi^{*}(\mathbf{r}, s_{m}^{+}) \phi(\mathbf{r}, s_{m}^{-}) \psi^{*}(\mathbf{r}) \right)$$

$$+ \sum_{m=1}^{M} \int d\mathbf{r} \, \phi^{*}(\mathbf{r}, s_{m}^{+}) \phi(\mathbf{r}, s_{m}^{-})$$

$$- \int d\mathbf{r} \, \phi^{*}(\mathbf{r}, 0) - n \ln \left(\frac{1}{V} \int d\mathbf{r} \, \phi(\mathbf{r}, N) \right). \tag{9}$$

The partition function in Eq. (7) must be multiplied by M more factors of Z_0 in this alternative canonical ensemble. For continuous Gaussian chains, this representation is better suited for analytical analysis, as we will show.

The general theory outlined above exactly enumerates all of the reaction products, including both tree-like and looped networks. A Taylor series representation of the partition function Z in the fields ϕ , ϕ^* , ψ , and ψ^* generates terms corresponding to all possible sets of molecules, which can be conveniently represented by standard Feynman diagrams. Both the discrete chain and continuous chain models can be numerically simulated without approximation using a complex Langevin scheme, where field configurations are evolved stochastically over fictitious time. Numerical methods for complex Langevin simulations can be found in Refs. 28 and 38. An approximate treatment of the field theory at the mean-field level does not

account for any looped structures, generating only tree-like networks. In the following section, we will explore the thermodynamic implications of the mean-field treatment of our theory.

III. RESULTS AND DISCUSSION

For the rest of the work, we will use the continuous chain theory in the alternative canonical ensemble described in the previous section and simplify the theory by considering contact interactions and bonding, such that $u(\mathbf{r}, \mathbf{r}') = u_0 \delta(\mathbf{r} - \mathbf{r}')$ and $R(\mathbf{r}, \mathbf{r}') = \delta(\mathbf{r} - \mathbf{r}')$. Note that all of the main results can also be obtained with the discrete chain theory.

A. Mean-field theory

A natural place to start is the mean-field limit of the theory, corresponding to saddle-point configurations of the fields that satisfy

$$\frac{\delta H}{\delta \phi^*(\mathbf{r}, s)} = \frac{\delta H}{\delta \phi(\mathbf{r}, s)} = \frac{\delta H}{\delta \psi^*(\mathbf{r})} = \frac{\delta H}{\delta \psi(\mathbf{r})} = 0.$$
 (10)

The functional derivatives in Eq. (10) yield configurations that in unbound space are homogeneous in the spatial dimension but inhomogeneous in the contour variable. The point-like description of reactive sites along with the causal response in ϕ^* and ϕ require careful mathematical treatment when taking variations of the Hamiltonian. Full expressions for the saddle-point configurations can be found in the Appendix. The mean-field analysis shows the ψ and ψ^* fields are connected to meaningful quantities. Their product gives the density of functional groups, $\psi^*\psi=MC$, the number density of bonds is $\rho_{\rm bond}=\lambda\psi^2/2$ as follows from Eq. (6), and the conversion is given by

$$\eta = \frac{\lambda \psi^2}{MC} = \frac{1 + 2\lambda MC - \sqrt{1 + 4\lambda MC}}{2\lambda MC}.$$
 (11)

The conversion scales as $\eta \sim \lambda MC$ and $\eta \sim 1 - (\lambda MC)^{-1/2}$ for small and large λMC , respectively.

The mean-field Helmholtz free energy of the system can be found through substitution of the mean-field conditions into the effective Hamiltonian in the partition function,

$$F/\bar{V} = C \ln{(C)} - C + \frac{1}{2}BC^2 + \frac{1}{2}MC\eta + MC \ln{(1-\eta)},$$
 (12)

where we have introduced the scaled parameter $B = u_0 N^2 / R_{g_0}^3$. The fourth and fifth terms account for the reversible reactions. For M=0, the free energy reduces to that of a polymer solution with excluded volume interactions. Equation (12) is equivalent to the free energy derived by Semenov and Rubinstein in Ref. 19 and the mean-field free energy of M-arm stars with reactive ends.³⁹ At the mean-field level, chain structure is neglected, so one would expect the same result for different architectures. Accordingly, the discrete chain theory in Eq. (5) results in the same mean-field free energy. The osmotic pressure also contains an explicit term related to the conversion,

$$\Pi = C + \frac{1}{2}BC^2 - \frac{1}{2}MC\eta. \tag{13}$$

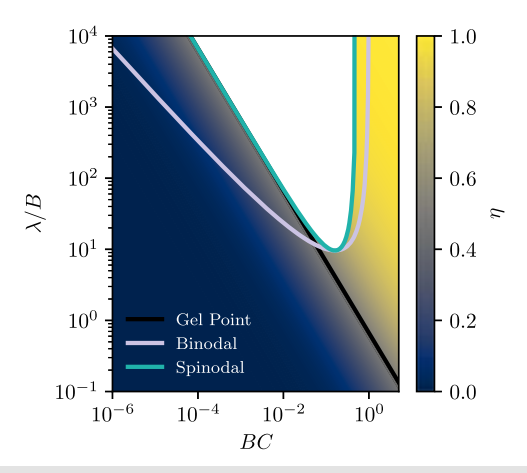


FIG. 2. Sol–gel phase diagram for M=3. The colorbar indicates conversion, η . The gel point corresponds to the Flory gel point, $\eta_c=\frac{1}{M-1}$.

By chemical potential and osmotic pressure equivalence, the mean-field phase behavior is fully described by three parameters—BC, λ/B , and M. The spinodal corresponds to the condition

$$\frac{1+\eta}{\eta} = \frac{M BC}{1+BC}. (14)$$

Figure 2 shows the sol–gel phase diagram for M=3. Phase separation only occurs for sufficiently high λ/B , which represents the competition between the attraction of the reactive sites and repulsion from the excluded volume. The gel point indicated in the diagram represents the critical conversion from Flory, 9 $\eta_c=1/(M-1)$. The binodal envelope provides the locus of coexisting dilute (sol) and concentrated (gel) phases for each value of λ/B in the two phase region. The macrophase spinodal approaches the gel point at low values of BC, indicating that the sol–gel transition coincides with gel formation. For higher solvent quality or higher concentration, a disordered homogeneous gel may form above the gel point but outside of the spinodal region. While not shown, increasing M lowers the energy necessary to form a gel, broadening the overall 2-phase region.

B. Disordered phase structure and stability

Mean-field theory neglects correlations so that any effect of reactive site sequence or position does not affect the thermodynamics. The RPA provides further information on the disordered structure and stability of the disordered phase under the mean-field approximation. The RPA amounts to a weak inhomogeneity expansion around the saddle-point configurations and serves to capture linear response behavior. Using the procedure outlined in Ref. 27, we apply a weak perturbative field $J(\mathbf{r})$ that is coupled to the polymer density to obtain the perturbed Hamiltonian, $H_J = H + \int d\mathbf{r} J(\mathbf{r}) \tilde{\rho}(\mathbf{r})$. Expanding each of the fields to first order in J allows us to calculate the response function,

$$\delta \hat{\tilde{\rho}}(\mathbf{k}) = -S(\mathbf{k})\hat{J}(\mathbf{k}),$$
 (15)

where $\delta \hat{\rho}(\mathbf{k})$ is the Fourier transform of the first-order density response, $S(\mathbf{k})$ is the static structure factor, and $\hat{f}(\mathbf{k})$ is the Fourier transform of the weak perturbative field. The static structure factor is typically represented as

$$S(\mathbf{k}) = \frac{\rho_0 NG(\mathbf{k}; \{\alpha\}, N)}{1 + u_0 \rho_0 NG(\mathbf{k}; \{\alpha\}, N)},$$
(16)

where $\rho_0 = NC$ is the reduced monomer density and $G(\mathbf{k}; \{\alpha\}, N)$ is the scattering function for a single polymer chain. For an ideal Gaussian chain with no reactions, G is simply the Debye scattering function, $g_D(x) = \frac{2}{x^2}(e^{-x} + x - 1)$ with $x = k^2 R_{g_0}^2$ and $k^2 = |\mathbf{k}|^2$. The general expression is

$$G(\mathbf{k}; \{\alpha\}, N) = g_D(x) + P(x; \{\alpha\}, \eta), \tag{17}$$

where the second term accounts for the correlations contributed by the larger polymer species created by the reversible bonding reactions,

$$P(x; \{\alpha\}, \eta) = \frac{\frac{\eta}{M} \left(\sum_{j=1}^{M} \left[r(x, N, s_j) + r(x, s_j, 0) \right] \right)^2}{1 - \frac{\eta}{M} \sum_{j=1}^{M} \left(\sum_{m=1}^{M} e^{-x|s_j - s_m|/N} - 1 \right)},$$
 (18)

with $r(x; s, s') = \frac{1}{x} \left(1 - e^{-x(s-s')/N}\right)$. An important feature of Eq. (17) is that the conversion η appears explicitly in the additive term $P(x; \{\alpha\}, \eta)$, allowing us to directly analyze the effects of reversible bonding on the structure factor. Practically speaking, such a compact analytical form for the static structure factor stems from the convenience that all reactivity information is embedded in the ψ and ψ^* fields. The structure factor for discrete chains can be found with the same approach and is given in the Appendix, yielding a similarly compact expression. Finally, we note that Eq. (18) enumerates only tree-like reaction products, which is a consequence of the mean-field approximation. The full theory accounts for additional ring and loop structures among the sol and gel components.

The limit of $S^{-1}(0)$ gives a measure of the average molecular weight, N_w ,

$$\frac{1}{S(0)} = \frac{1}{\rho_0 N_w} + u_0,\tag{19}$$

yielding

$$N_w/N = G(0; \{\alpha\}, N) = \frac{1+\eta}{1-(M-1)\eta}.$$
 (20)

The average molecular weight diverges for a critical conversion of $\eta_c = 1/(M-1)$, which is consistent with classical gelation theory that includes only tree-like polymer structures. As expected, N_w does not depend on the specific placement of reactive sites.

With a large design space for supramolecular polymers, Eq. (17) can be used to probe the structure of disordered systems. We will consider a few specific cases below. For a single reactive group at position s_1 , we obtain

$$G(\mathbf{k}; s_1, N) = g_D(x) + \eta (r(x, s_1, 0) + r(x, N, s_1))^2.$$
 (21)

In the limit of $\eta \to 1$ when $s_1 = N/2$, the scattering function is equivalent to that of a 4-arm star with each arm having degree of

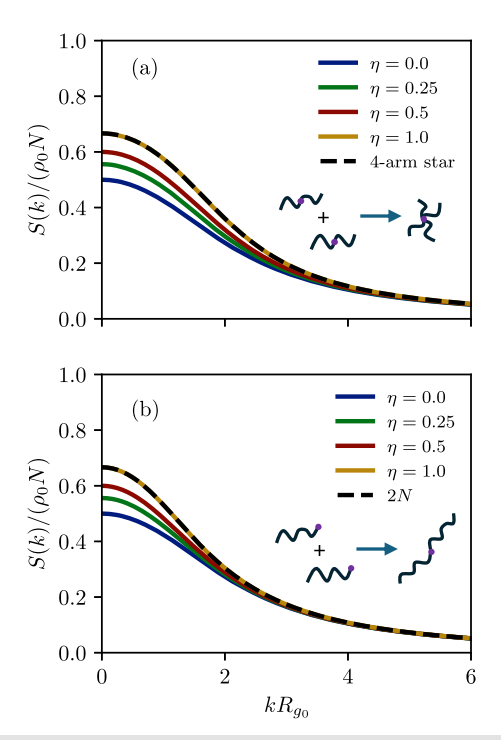


FIG. 3. Structure factor as a function of conversion for simple architectures with M=1 and $BC=u_0\rho_0N=1$. The functional group is placed (a) in the center and (b) at the end of the chain. See Ref. 40 for the structure factor of a star polymer.

polymerization N/2. Likewise, full conversion with $s_1 = 0$ (or $s_1 = N$) gives the scattering function for a linear polymer of length 2N. We show these comparisons numerically in Fig. 3.

For M=2, in the telechelic limit $(s_1 \to 0 \text{ and } s_2 \to N)$, the scattering function is

$$G(\mathbf{k}; \{0, N\}, N) = g_D(x) + r(x; N, 0)^2 \frac{2\eta}{1 - ne^{-x}}.$$
 (22)

The result mentioned above is in agreement with Ref. 27; however, the expression here is notably easier to interpret since η naturally arises in the RPA.

A final case we will consider is that of a linear polymer with a multi-functional end group, where M reactive sites reside at the same contour position. The scattering function reduces to

$$G(\mathbf{k}; \{0\}, N) = g_D(x) + r(x; N, 0)^2 \frac{M\eta}{1 - (M - 1)\eta}.$$
 (23)

C. Microstructured gels

From the response function, we can determine the stability of the disordered phase. The onset of a divergence in the static structure factor $[S^{-1}(\mathbf{k}^*)=0]$ indicates the stability limit of the homogeneous disordered phase. When $\mathbf{k}^*=0$, the system undergoes macrophase separation, while $\mathbf{k}^*>0$ indicates phase separation into a microstructured phase with characteristic length scale

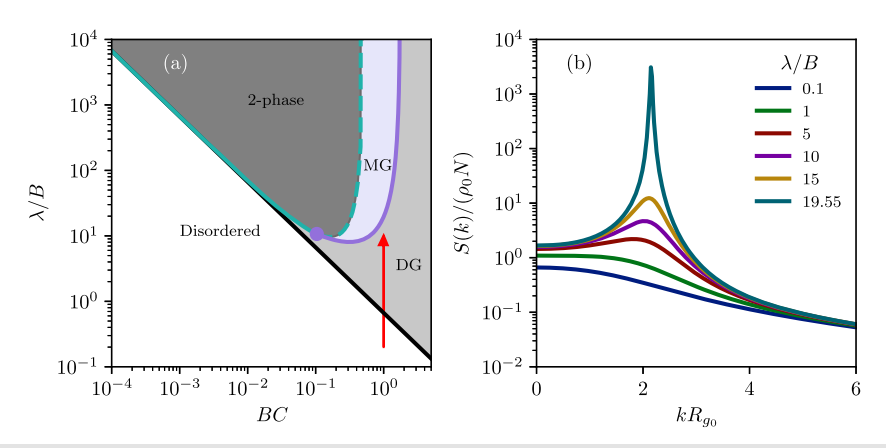


FIG. 4. (a) Sol-gel phase diagram with microphase region for M=3. DG = Disordered Gel, MG = Microstructured Gel. Reactive sites are at positions $s_{\alpha}/N \in \{9/20, 1/2, 11/20\}$. The green dashed line is a continuation of the macrophase stability boundary from the Lifshitz point (purple circle). (b) Instability in the structure factor along the arrow path in (a).

 $D^*=2\pi/|\mathbf{k}^*|$. An advantage of our current theory is that we can explore arbitrary numbers and sequences of reactive sites. Interestingly, we observe a sequence-dependent microstructured gel phase that, to the best of our knowledge, has not been previously reported for neutral gels. Figure 4(a) shows a representative phase diagram for M=3 with a reactive site sequence of $s_\alpha/N \in \{9/20,1/2,11/20\}$. This sequence corresponds to placing a reactive site in the center of the polymer chain with reactive sites spaced $\Delta s=N/20$ on each side. Figure 4(b) shows the divergence in the structure factor at $k^*R_{g_0}\approx 2.2$ upon approaching the spinodal. The boundary of the microphase region terminates at a Lifshitz point (purple circle), where the microphase spinodal intersects the macrophase spinodal and D^* diverges.

The microstructured region of the phase diagram is sequencedependent since spacing between reactive sites significantly affects the width of the microphase region. Figure 5 shows the phase

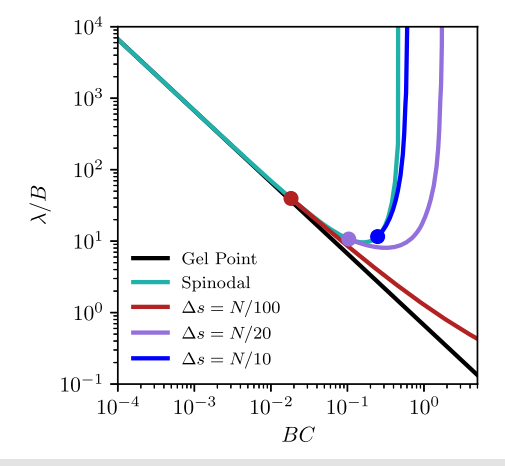


FIG. 5. Effect of reactive site spacing on the extent of the microphase region for M=3. Values of Δs correspond to the placement of $s_{\alpha}/N \in \{1/2 - \Delta s/N, 1/2, 1/2 + \Delta s/N\}$.

diagram for different reactive site spacing. Increasing Δs narrows the microphase region. For the smallest spacing ($\Delta s = N/100$), the microphase boundary approaches the gel point. That is, the microphase is stabilized as soon as the system forms a gel. We can understand the effect of spacing by using the Lifshitz point. The value of BC at the Lifshitz point, denoted $(BC)_L$, indicates the prevalence of the microphase in the phase diagram. Lower values of (BC)_L correspond to a wider microphase region, as evident in Fig. 5. D* decreases away from the Lifshitz point. For the same value of BC in Fig. 5, the characteristic length scale of the microphase region decreases with decreasing Δs . Larger values of Δs require sections of the chain between reactive sites to organize into a polymer-rich phase, whereas smaller values of Δs presumably allow longer sections of the chain to remain extended in solvent. Later in this section, we will further explore the physical origin of the microphase.

Due to the pliability of the structure factor in our theory, we can analytically obtain the Lifshitz point for M = 3. Notably, the microphase is only present for M > 2. In principle, one can obtain the Lifshitz point for any value of M > 2; however, for conciseness, we only present M = 3. $(BC)_L = y$ is the physical root of the quadratic equation

$$2(y+1)((y-2)s_1/N + 3ys_2(1-s_2/N) + (5y+2)s_3/N -3y(s_1/N)^2 - 3y(s_3/N)^2) - 3y(2y+3) = 0.$$
 (24)

The placement of reactive sites influences the prevalence of the microphase region, but what is the physical origin of a microstructured gel? The microphase corresponds to heterogeneity in the gel structure caused by local clustering of bonds. Using the RPA, we can evaluate bond-bond correlations from the response to a weak perturbation $J_{\rm bond}(\mathbf{r})$,

$$\delta \hat{\rho}_{\text{bond}}(\mathbf{k}) = -S_{\text{bond}}(\mathbf{k})\hat{J}_{\text{bond}}(\mathbf{k}),$$
 (25)

where $\delta \hat{\rho}_{bond}(\mathbf{k})$ is the first order bond density fluctuation. Figure 8 shows that the length scale of the instability aligns with that of the

instability in Fig. 4, suggesting ordering of bonds drives finite wavelength instabilities in segment density. Since the microstructured region of the phase diagram lies above the gel point, the clusters of bonds are not isolated but likely manifest as reactive-site-rich, globular regions within the gel alongside pockets of solvent. Such a physical picture is similar to that of a gel with spatial inhomogeneities discussed elsewhere in polymer gel literature. 41,42

Gels with heterogeneous structure are usually associated with charged gels.⁴³ Bonding between reactive sites tends to cause macrophase separation since the favorable bond energy produces attractive interactions similar to the effect of lowering the solvent quality, as seen in the negative contribution to the osmotic pressure [Eq. (13)]. In weakly charged gels with marginal to poor solvent conditions, the solvent-induced tendency for macrophase separation competes with segment-level electrostatic repulsion, leading to phase separation at finite **k**. Rabin and Panyukov^{44,45} showed that electrostatic correlation at the Debye–Hückel level naturally renormalizes the excluded volume parameter, enabling prediction of microphase separation. Similarly, the static structure factor in Eq. (17) can be written as

$$S(\mathbf{k}) = \frac{\rho_0 N g_D(x)}{1 + \tilde{u}(x)\rho_0 N g_D(x)},$$
(26)

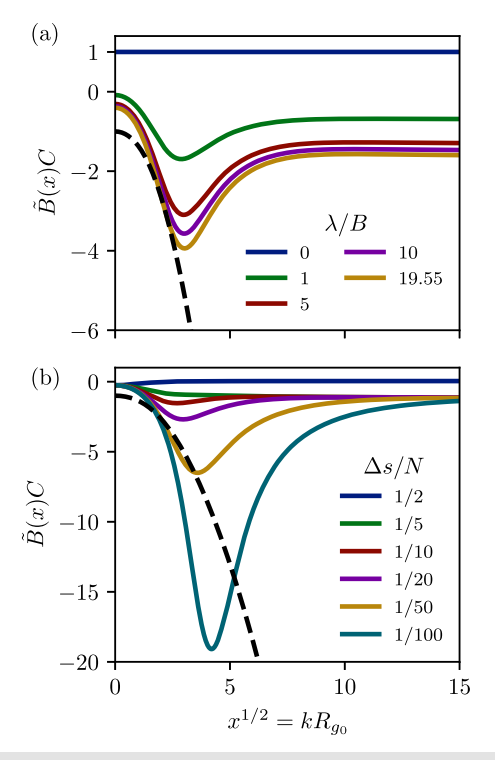


FIG. 6. Renormalized excluded volume parameter $\tilde{B}(x)=N^2\tilde{u}(x)/R_{g_0}^3$ for (a) constant spacing of $\Delta s=N/20$ and varying λ/B and (b) constant $\lambda/B=3$ with varying spacing. The bare excluded volume is BC=1. Values of Δs correspond to the placement of $s_\alpha/N\in\{1/2-\Delta s/N,1/2,1/2+\Delta s/N\}$. The dashed line is $-g_D(x)$, where the intersection of $\tilde{B}(x)C=-g_D(x)$ corresponds to $S^{-1}(\mathbf{k})=0$.

where $\tilde{u}(x)$ is a renormalized excluded volume parameter of the form

$$\tilde{u}(x) = u_0 - \frac{1}{\rho_0 N g_D(x)} \frac{P(x; \{\alpha\}, \eta) / g_D(x)}{1 + P(x; \{\alpha\}, \eta) / g_D(x)}.$$
 (27)

The perturbation to u_0 is strictly negative so that the reversible bonding effectively decreases solvent quality.

Of interest is how this effective solvent quality is dependent on the placement of reactive sites. Because $P(x; \{\alpha\}, \eta)$ includes correlations between reactive sites, the position/sequence of reactive sites will influence the solvent quality. Figure 6 quantifies the effect of sequence on the parameter $\tilde{B}(x) = N^2 \tilde{u}(x)/R_{g_0}^3$. Figure 6(a) shows for a fixed sequence of $s_\alpha/N \in \{9/20, 1/2, 11/20\}$ that increasing the bond energy (increasing conversion) lowers the effective solvent quality non-uniformly with the wavevector. Approaching the microphase spinodal ($\lambda/B \approx 19.55$), the solvent quality intersects the dashed black line, indicating phase separation $[\tilde{B}(x)C = -1/g_D(x)]$. Clearly, the effective solvent quality is non-uniform over k, and phase separation requires a sufficiently poor solvent. For a constant value of $\lambda/B = 3$, Fig. 6(b) highlights the effect of sequence. The foremost observation is that small spacing between monomers significantly decreases $\tilde{B}(x)C$. More subtly, the wavevector of minimum $\tilde{B}(x)C$ depends on the spacing. Closer spacing of reactive sites induces stronger segment-level attraction through correlations between sites. When the induced attraction is sufficiently large, microphase separation occurs.

From the discussion earlier, the characteristic length scale of the domains formed by microphase formation is a non-trivial balance between the total correlation function of the segments composing the polymer network and the correlations between reactive sites. We can further probe this balance by numerically evaluating the domain spacing over different values of BC, M and reactive site spacing Δs (Fig. 7). Note that λ/B for the microphase is determined by the stability boundary and is not independent of the other parameters.

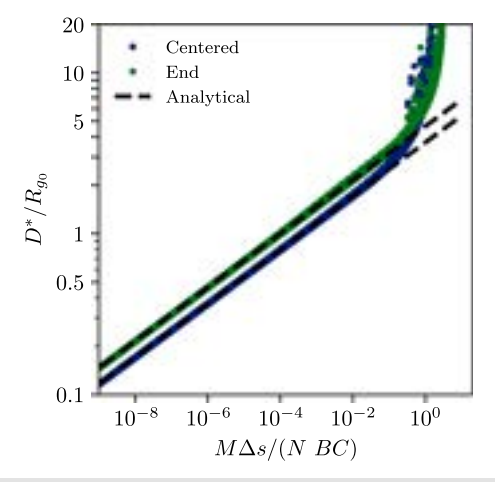


FIG. 7. Characteristic length scale $(D^* = 2\pi/|\mathbf{k}^*|)$ of microstructured gel phase vs a combined variable $\frac{M\Delta s}{NBC}$. "Centered" and "End" correspond to reactive-site positions centered in the middle of the chain or originating from the end of the chain with spacing Δs , respectively. The ranges of the parameters to generate the points in the plot are $BC \in [10^{-4}, 2]$, $M \in [3, 100]$, $M\Delta s/N \in [10^{-9}, 1]$. Analytical results are from Eq. (28) for each sequence type.

Analytically, we approximate the domain size from an asymptotic analysis of the structure factor obtained from the RPA. For $|\mathbf{k}|^* \gg 1$ and $\Delta s/N \ll 1$, corresponding to small domain sizes and small reactive site spacing, we find that the domain size is approximately

$$D^* \approx \alpha R_{g_0} \left(\frac{M^2 - 1}{M} \frac{\Delta s}{N BC} \right)^{1/6} \sim R_{g_0} \left(\frac{M \Delta s}{N BC} \right)^{1/6}, \quad (28)$$

where $\alpha = 2^{5/6}\pi/3^{1/6}$ and $2^{1/2}\pi/3^{1/6}$ for end and center sequences, respectively. "End" and "centered" sequences correspond to reactive-site positions centered in the middle of the chain or originating from the end of the chain with precise spacing Δs . From Fig. 7, we see that the scaling relationship is valid until $\frac{M\Delta s}{RC} < 1$, above which the domain size begins to diverge approaching the Lifshitz point. Comparing the two types of sequences considered, the domain spacing is larger when the reactive sites are placed at the end of the chain compared to the center. This implies that the length of the long, unreactive portion of the chain plays a role in the domain scale of the microphase that forms. Increasing BC reduces domain size since the attraction from reactive sites cannot compensate additional repulsion from excluded volume interactions, which break associations in the microdomain in favor of a disordered network. The scaling relationship uncovers this balance and points to design variables that can be used to tune the domain size.

IV. CONCLUSION

Supramolecular polymers are an attractive class of materials for their tunability and reversible interactions; however, their ability to form associations requires a unique theoretical treatment. The coherent states framework allows us to construct field theories that capture the complexity of reaction products that arise from supramolecular interactions in a way that can be analyzed with both analytical methods and direct numerical simulation.

The current work extends coherent states theories for supramolecular polymers to a wider array of architectures. The most compelling aspect of our approach is the realization that, irrespective of architecture, reactive sites can be tagged with a field marker ψ^* that enables complex macromolecular reaction products to be readily and exactly enumerated. Because of its simplicity, this approach can trivially be extended to multi-component and multi-reaction systems with the addition of ψ^* fields for each type of reacting component. Since ψ and ψ^* are connected to each of the reacting beads/species, accessing thermodynamic quantities related to the extent of the various reactions is straightforward. Moreover, the modified coherent states framework enables ready access to analytical mean-field solutions and RPA structure factors and stability limits.

As demonstrated in the results, our theory unearths novel thermodynamics, even in a well-studied one-component system. In particular, the presence of a microstructured gel was found to be dependent on the spacing and placement of reactive sites. Sufficiently close spacing of reactive sites along the backbone pushes the microphase spinodal toward the gel point. For many years, authors have noted there is no thermodynamic transition at the gel point for a neutral polymer in a good solvent, whereas our results show that gelation can be accompanied by microphase separation for chains

with closely clustered stickers. The microstructured gel results from the attractive polymer–polymer correlations arising from nonuniform sticker placement. The appearance of a microphase in a one-component system suggests multi-component supramolecular systems may possess similar microphases, even for chemically similar polymers ($\chi=0$). For hetero-associating polymers, microstructured gels have been reported, but only for chemically dissimilar polymers. While our results are shown for continuous Gaussian chains, the general theory presented for discrete Gaussian chains can be used to construct polymers with varying monomer types, akin to sequenced-based biological polymers. There are undoubtedly rich thermodynamic phenomena yet to be found in supramolecular polymers, and the coherent states framework will likely play an important role in uncovering them.

ACKNOWLEDGMENTS

The authors acknowledge support of this work from the National Science Foundation through Grant No. DMR-2104255. Use was made of the BioPACIFIC Materials Innovation Platform computing resources of the National Science Foundation Award No. DMR-1933487, as well as computational facilities purchased with funds from the National Science Foundation (Grant No. CNS-1725797) and administered by the Center for Scientific Computing (CSC). The CSC is supported by the California NanoSystems Institute and the Materials Research Science and Engineering Center (MRSEC; NSF Grant No. DMR 2308708) at UC Santa Barbara.

AUTHOR DECLARATIONS

Conflict of Interest

The authors have no conflicts to disclose.

Author Contributions

Christopher Balzer: Conceptualization (equal); Writing – original draft (equal); Writing – review & editing (equal). **Glenn H. Fredrickson:** Conceptualization (equal); Writing – review & editing (equal).

DATA AVAILABILITY

The data that support the findings of this study are available from the corresponding author upon reasonable request.

APPENDIX A: VARIATIONS FOR CONTINUOUS CHAIN THEORY

The variations of the effective Hamiltonian with respect to each field in the alternative canonical ensemble with source/sink terms in Eq. (9) are given below. For ϕ^* and ϕ ,

$$\frac{\delta H}{\delta \phi^{*}(\mathbf{r}, s)} = \mathcal{L}\phi(\mathbf{r}, s) + \phi(\mathbf{r}, s) \int d\mathbf{r}' \ u(\mathbf{r}, \mathbf{r}') \tilde{\rho}(\mathbf{r}')$$

$$- n \sum_{m=1}^{M} \frac{\phi(\mathbf{r}, s_{m}^{-}) \psi^{*}(\mathbf{r}) \delta(s - s_{m})}{\int d\mathbf{r}' \ \phi^{*}(\mathbf{r}', s_{m}^{+}) \phi(\mathbf{r}', s_{m}^{-}) \psi^{*}(\mathbf{r}')}$$

$$- \delta(s) + \sum_{m=1}^{M} \phi(\mathbf{r}, s_{m}^{-}) \delta(s - s_{m}), \tag{A1}$$

$$\frac{\delta H}{\delta \phi(\mathbf{r}, s)} = \mathcal{L}^{\dagger} \phi^{*}(\mathbf{r}, s) + \phi^{*}(\mathbf{r}, s) \int d\mathbf{r}' \ u(\mathbf{r}, \mathbf{r}') \bar{\rho}(\mathbf{r}')$$

$$- n \sum_{m=1}^{M} \frac{\phi^{*}(\mathbf{r}, s_{m}^{+}) \psi^{*}(\mathbf{r}) \delta(s - s_{m})}{\int d\mathbf{r}' \ \phi^{*}(\mathbf{r}', s_{m}^{+}) \phi(\mathbf{r}', s_{m}^{-}) \psi^{*}(\mathbf{r}')}$$

$$- n \frac{\delta(s - N)}{\int d\mathbf{r}' \phi(\mathbf{r}, N)} + \sum_{m=1}^{M} \phi^{*}(\mathbf{r}, s_{m}^{+}) \delta(s - s_{m}), \quad (A2)$$

where $\mathcal{L}^{\dagger} = -\partial/\partial s - (b/6)\nabla^2$ is the adjoint of the chain diffusion operator. For ψ^* and ψ ,

$$\frac{\delta H}{\delta \psi^*(\mathbf{r})} = \psi(\mathbf{r}) - \sum_{m=1}^{M} \frac{\phi^*(\mathbf{r}, s_m^+) \phi(\mathbf{r}, s_m^-) \delta(s - s_m)}{\int d\mathbf{r}' \ \phi^*(\mathbf{r}', s_m^+) \phi(\mathbf{r}', s_m^-) \psi^*(\mathbf{r}')}, \quad (A3)$$

$$\frac{\delta H}{\delta \psi(\mathbf{r})} = \psi^*(\mathbf{r}) - 1 - \lambda \int d\mathbf{r}' \ R(\mathbf{r}, \mathbf{r}') \psi(\mathbf{r}'). \tag{A4}$$

Note that the ϕ^* and ϕ fields are evaluated with arguments ahead and behind the contour points s_m , respectively, in the variations. This has implications when integrating the variations above with respect to the contour variable, as is performed in obtaining mean-field configurations. Specifically, integration with respect to the contour variable introduces Heaviside functions whose argument depends on whether the integration direction comes from above or below a particular reactive site position s_m .

1. Mean-field configurations

The mean-field approximation is implemented by equating the variational derivatives in Eqs. (A1)–(A4) to zero. In unbound space, the ϕ and ϕ^* fields are functions of the contour variable, while ψ and ψ^* are uniform. Integrating the equations obtained from Eqs. (A1) and (A2) produces the mean-field configurations of ϕ and ϕ^* ,

$$\phi_0(s) = \frac{Ce^{-BC\frac{s}{N}}}{\phi_0^*(0)}\Theta(s), \tag{A5}$$

$$\phi_0^*(s) = \frac{Ce^{-BC\frac{(N-s)}{N}}}{\phi_0(N)}\Theta(N-s),$$
(A6)

where the "0" subscript indicates that the mean-field configuration of the field and $\Theta(x)$ is the Heaviside step function. An important relation is that $\phi_0^*(s)\phi_0(s) = \phi_0^*(s_m^+)\phi_0(s_m^-) = C$, where s_m is the position of a reactive site. Setting Eqs. (A3) and (A4) to zero produces a quadratic equation with a physical solution for the fields,

$$\psi_0^* = \frac{\sqrt{4\lambda MC + 1} + 1}{2},\tag{A7}$$

$$\psi_0 = \frac{\sqrt{4\lambda MC + 1} - 1}{2\lambda}.$$
 (A8)

APPENDIX B: STRUCTURE FACTOR FOR DISCRETE CHAINS

For discrete chains, the structure factor is

$$S(\mathbf{k}) = \frac{\rho_0 NG(\mathbf{k}; \{\alpha\}, N)}{1 + u_0 \rho_0 NG(\mathbf{k}; \{\alpha\}, N)}.$$
 (B1)

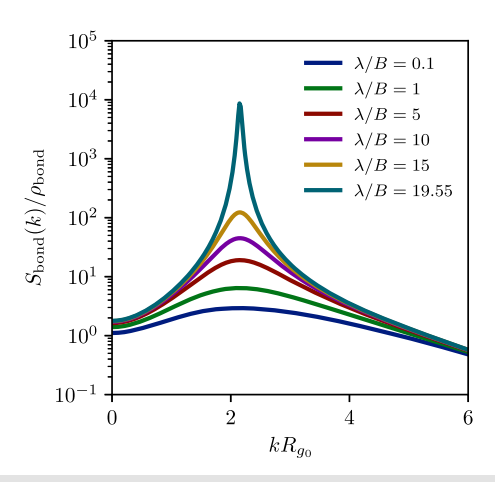


FIG. 8. Structure factor related to bond–bond correlation for the same conditions as that of Fig. 4. Note that the structure factor diverges at the same value of kR_{g_0} as that of Fig. 4.

The corresponding scattering function is

$$G(\mathbf{k}; \{\alpha\}, N) = g_{DD}(\mathbf{k}; N) + P_D(\mathbf{k}, \{\alpha\}, \eta), \tag{B2}$$

with

$$P_D(\mathbf{k}, \{\alpha\}, \eta) = \frac{\frac{\eta}{M} \left(\frac{1}{N} \sum_{m=1}^{N} \sum_{k=1}^{M} \hat{\Phi}(\mathbf{k})^{|\alpha_k - m|}\right)^2}{1 - \frac{\eta}{M} \sum_{k=1}^{M} \left(\sum_{m=1}^{M} \hat{\Phi}(\mathbf{k})^{|\alpha_k - \alpha_m|} - 1\right)},$$
(B3)

where $g_{DD}(\mathbf{k}; N) = \frac{N(1-\Phi(\mathbf{k})^2)+2\Phi(\mathbf{k})(\Phi(\mathbf{k})^N-1)}{N^2(1-\Phi(\mathbf{k}))^2}$ is the discrete Debye scattering function and $\hat{\Phi}(\mathbf{k})$ is the Fourier transform of the discrete chain bonding potential.

APPENDIX C: BOND CORRELATION

Figure 8 shows the structure factor related to bond-bond correlation for the same conditions as that of Fig. 4.

REFERENCES

¹T. F. A. de Greef and E. W. Meijer, Nature **453**, 171 (2008).

²T. Aida and E. Meijer, Isr. J. Chem. **60**, 33 (2020).

³H.-Q. Peng, W. Zhu, W.-J. Guo, Q. Li, S. Ma, C. Bucher, B. Liu, X. Ji, F. Huang, and J. L. Sessler, Prog. Polym. Sci. 137, 101635 (2023).

⁴R. Dong, Y. Zhou, and X. Zhu, Acc. Chem. Res. 47, 2006 (2014).

⁵R. Dong, Y. Zhou, X. Huang, X. Zhu, Y. Lu, and J. Shen, Adv. Mater. 27, 498 (2015).

⁶F. Huang and O. A. Scherman, Chem. Soc. Rev. **41**, 5879 (2012).

⁷P. K. Hashim, J. Bergueiro, E. W. Meijer, and T. Aida, Prog. Polym. Sci. 105, 101250 (2020).

⁸ A. D. O'Donnell, S. Salimi, L. R. Hart, T. S. Babra, B. W. Greenland, and W. Hayes, React. Funct. Polym. **172**, 105209 (2022).

⁹P. J. Flory, J. Am. Chem. Soc. **63**, 3083 (1941).

¹⁰W. H. Stockmayer, J. Chem. Phys. **11**, 45 (1943).

¹¹P. J. Flory and J. Rehner, Jr., J. Chem. Phys. **11**, 521 (1943).

¹²T. Tanaka, D. Fillmore, S.-T. Sun, I. Nishio, G. Swislow, and A. Shah, Phys. Rev. Lett. 45, 1636 (1980).

- ¹³ M. S. Dimitriyev, Y.-W. Chang, P. M. Goldbart, and A. Fernández-Nieves, Nano Futures 3, 042001 (2019).
- ¹⁴Y. Rabin and S. Panyukov, J. Comput.-Aided Mater. Des. 3, 281 (1996).
- ¹⁵W. Hong, X. Zhao, J. Zhou, and Z. Suo, J. Mech. Phys. Solids 56, 1779 (2008).
- ¹⁶ A. K. Omar and Z.-G. Wang, Phys. Rev. Lett. **119**, 117801 (2017).
- ¹⁷Y. An, F. J. Solis, and H. Jiang, J. Mech. Phys. Solids **58**, 2083 (2010).
- ¹⁸D. Jia and M. Muthukumar, Gels 7, 49 (2021).
- ¹⁹ A. N. Semenov and M. Rubinstein, Macromolecules 31, 1373 (1998).
- ²⁰S. P. O. Danielsen, Macromolecules **56**, 6527 (2023).
- ²¹ A. Mohan, R. Elliot, and G. H. Fredrickson, J. Chem. Phys. **133**, 174903 (2010).
- ²²Z. Mester, A. Mohan, and G. H. Fredrickson, Macromolecules 44, 9411 (2011).
- ²³S. Panyukov and Y. Rabin, Phys. Rep. **269**, 1 (1996).
- ²⁴S. F. Edwards and K. F. Freed, J. Phys. C: Solid State Phys. 3, 739 (1970).
- ²⁵S. F. Edwards and K. F. Freed, J. Phys. C: Solid State Phys. 3, 750 (1970).
- ²⁶S. F. Edwards and K. F. Freed, J. Phys. C: Solid State Phys. **3**, 760 (1970).
- ²⁷G. H. Fredrickson and K. T. Delaney, J. Chem. Phys. **148**, 204904 (2018).
- ²⁸G. H. Fredrickson and K. T. Delaney, Field-Theoretic Simulations in Soft Matter and Quantum Fluids, 1st ed. (Oxford University Press, Oxford, 2023).
- ²⁹D. L. Vigil, A. Zhang, K. T. Delaney, and G. H. Fredrickson, Macromolecules 56, 9994 (2023).
- 30 A. Kulshreshtha, R. C. Hayward, and A. Jayaraman, Macromolecules 55, 2675 (2022).

- ³¹Z. Wu, J. W. Wu, Q. Michaudel, and A. Jayaraman, Macromolecules **56**, 5033 (2023).
- ³²Z. Huang, B. B. Noble, N. Corrigan, Y. Chu, K. Satoh, D. S. Thomas, C. J. Hawker, G. Moad, M. Kamigaito, M. L. Coote, C. Boyer, and J. Xu, J. Am. Chem. Soc. 140, 13392 (2018).
- $^{\bf 33}$ B. R. Elling, J. K. Su, J. D. Feist, and Y. Xia, Chem 5, 2691 (2019).
- ³⁴G. H. Fredrickson, S. Xie, J. Edmund, M. L. Le, D. Sun, D. J. Grzetic, D. L. Vigil, K. T. Delaney, M. L. Chabinyc, and R. A. Segalman, ACS Polym. Au 2, 299 (2022).
- ³⁵O. A. Lee, M. K. McBride, M. Ticknor, J. Sharpes, and R. C. Hayward, Chem. Mater. 35, 10030 (2023).
- ³⁶B. Wang, Y. Mi, B. Wang, L. Pan, Y. Li, and D.-P. Song, Macromolecules 57, 1770 (2024).
- ³⁷J. G. Baker, R. Zhang, and C. A. Figg, J. Am. Chem. Soc. **146**, 106 (2024).
- ³⁸X. Man, K. T. Delaney, M. C. Villet, H. Orland, and G. H. Fredrickson, J. Chem. Phys. **140**, 024905 (2014).
- ³⁹D. Vigil, "Efficient field theoretic simulations of branched and network polymers," Ph.D. thesis, UC, Santa Barbara, 2023.
- ⁴⁰L. A. Molina, A. Rey, and J. J. Freire, Comput. Theor. Polym. Sci. 7, 243 (1997).
- ⁴¹ F. Ikkai and M. Shibayama, J. Polym. Sci., Part B: Polym. Phys. **43**, 617 (2005).
- ⁴²S. Seiffert, Polym. Chem. **8**, 4472 (2017).
- ⁴³M. Shibayama, Polym. J. **43**, 18 (2011).
- 44 Y. Rabin and S. Panyukov, Macromolecules 30, 301 (1997).
- 45 S. V. Panyukov, Polym. Sci., Ser. A 58, 886 (2016).